Acta Cryst. (1989). A**45**, 132-141

Grazing-Incidence Bragg–Laue X-ray Diffraction

BY STEPHEN M. DURBIN AND THOMAS GOG

Physics Department, Purdue University, West Lafayette, IN 47907, *USA*

(*Received* 30 *May* 1988; *accepted* 30 *August* 1988)

Abstract

Internal waves excited by the dynamical diffraction of X-rays from a single set of crystal planes perpendicular to the incidence surface can produce both Bragg diffracted and reflected beams *and* Laue diffracted and transmitted beams for crystal slabs of finite thickness. The excitation of Bragg and Laue beams for grazing-incidence diffraction geometries is investigated experimentally and theoretically. The traditional dispersion surface picture for describing allowed internal and external wave vectors is developed to illustrate how the Bragg and Laue beams arise. Experiments performed on a thin silicon wafer demonstrate the evolution of the Laue beams from the back surface into Bragg beams at the front surface of the crystal. The results are in good agreement with calculated curves obtained from the '*n*-beam' diffraction theory of Colella [*Acta Cryst.* (1974), A**30**, 413-423]. This theory is shown to be very useful for grazing-incidence excitations because of its completely general treatment of Bragg and Laue beams, and the exact numerical nature eliminates the need for approximations. Experiments also reveal how the presence of a 40 Å AuPd layer on the incidence surface suppresses the Bragg-diffracted beam but not the specular and Laue beams.

1. Introduction

The diffraction of X-rays from planes perpendicular to the surface of a flat semi-infinite crystal has received considerable attention in recent years because of the dominant role played by the surface in determining the directions and intensities of the diffracted beams (Baryshevskii, 1976; Andreev, Kov'ev, Matveev & Ponomarev, 1982; Afanas'ev & Melkonyan, 1983; Aleksandrov, Melkonyan & Stepanov, 1984; Cowan, 1985; Höche & Brümmer, 1986; Cowan, Brennan, Jach, Bedzyk & Materlik, 1986; Bernhard, Burkel, Gompper, Metzger, Peisl, Wagner & Wallner, 1987). For a plane-wave beam of X-rays incident at a grazing angle to a crystal surface and also satisfying the Bragg condition for diffracting from a reciprocal-lattice vector **H** parallel to that surface, the usual diffracted beam would be directed into the crystal if it were not for the slight change in the index of refraction at the surface. The diffracted beam is instead 'reflected' from the surface, in a manner similar to the specular reflection of the incident beam for grazing angles below the critical angle Φ_c for total reflection. The small increase in wavelength due to refraction therefore changes the scattering geometry from the Laue case, in which the diffracted X-rays travel into the crystal to form exit beams at the rear surface, to the Bragg case, where the diffracted beams are directed away from the front surface of the crystal.

The excitation of a reflected diffracted beam in grazing-incidence scattering geometries is easily explained. When the incident beam is at the critical angle Φ_c with respect to the crystal surface, the internal transmitted beam travels parallel to the interface with a wavelength slightly larger than the vacuum value, and is damped exponentially in the perpendicular direction. The specular reflected beam is generated because the incident beam alone cannot satisfy the requirements for phase continuity at the inter-

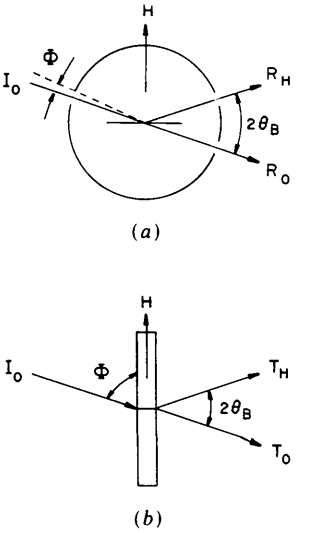

Fig. 1. Two views of diffraction from a reciprocal-lattice vector **H** in the surface plane of a crystalline wafer, illustrating how a single reflection can generate either Bragg or Laue beams. (*a*) For incident angle Φ less than the critical angle for total reflection Φ_c, the exit beams consist of the usual specular beam R_O plus a Bragg diffracted beam R_H. (*b*) Rotating the wafer about the vector **H** until Φ is much larger than Φ_c will result in the usual Laue diffracted beam T_H and the Laue forward-diffracted (transmitted) beam T_O. Here the wafer is viewed edge-on.

0108-7673/89/010132-10$03.00

face.* That is, two external waves are necessary to match the tangential components of the electric and magnetic fields with the one internal wave travelling parallel to the surface. If the crystal is then properly oriented so this internal wave can diffract from planes perpendicular to the surface, a diffracted wave will be excited which also travels parallel to the interface but deflected from the original wave's direction by twice the Bragg angle. Satisfying the boundary conditions for these two internal waves requires *three* external waves: the incident beam, a specular beam, and a Bragg-reflected diffraction beam.

The transition from Laue to Bragg scattering can be visualized by considering a thin parallel-sided slab (Figs. 1 and 2). If the incident beam is always maintained to diffract off **H** while the crystal is rotated about the φ axis parallel to the **H** vector,† the two Laue beams which exist for large angles of incidence will be transformed into a specular reflected beam and a reflected Bragg diffracted beam for grazing angles of incidence. This perspective suggests that internal waves which can couple to Laue beams are an integral aspect of surface diffraction. In this paper we discuss the theory of surface dynamical diffraction from this perspective, emphasizing the simultaneous excitation of strong Bragg and Laue beams from a single surface reflection **H**. A geometrical description of dynamical surface diffraction based on dispersion surfaces and exit spheres is described, and the results of synchrotron measurements of Bragg–Laue excitations from a silicon wafer are explained in terms of this geometrical picture. In addition, we compare these results with calculations performed using a completely general and *exact* procedure due to Colella (1974), in which no artificial distinctions are made between Bragg and Laue excitations. This program is shown to be very useful for surface dynamical diffraction.

* This is explained in many texts on electromagnetism (*e.g.* Lorrain & Corson, 1970).

† The angle φ about the **H** axis is not the same as the angle Φ between the incident beam and the surface. If the incident beam is at an angle θ with respect to the **H** crystal planes and the crystal surface is rotated about the **H** direction by φ (Fig. 2), then

$$\sin \Phi = \sin \varphi \cos \theta.$$

Upper-case angles Φ shall always refer to angles between a beam and the crystal surface, while lower-case angles φ are the equivalent rotation angles about the **H** axis. In experiments it is convenient to align the crystal with the **H** direction parallel to a particular diffractometer axis, *e.g.* the φ axis. Thus it is the angles φ and θ which are accurately known, permitting calculation of Φ. The various critical angles φ_c in the following refer to the equivalent rotations about the **H** axis corresponding to the true grazing angles Φ_c.

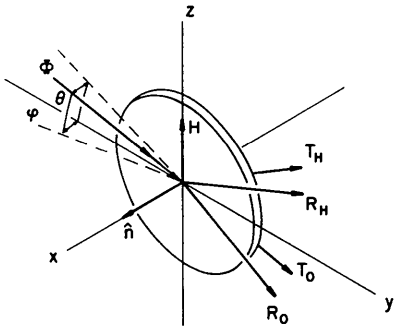

Fig. 2. For incident angles comparable to Φ_c, all four beams can exist with finite intensities determined by Φ and the thickness of the wafer. Note that Φ is the angle of incidence, while φ is the angle about the **H** axis through which the wafer has been rotated. The vector $\hat{\mathbf{n}}$ indicates the direction normal to the crystal surface.

II. Dynamical diffraction theory

One of the earliest published investigations of surface X-ray diffraction was by Marra, Eisenberger & Cho (1979), and a theoretical description using kinematic scattering was presented by Vineyard (1982). Discussions of the dynamical interaction of surface beams with perfect crystals have been published by Afanas'ev & Melkonyan (1983), Aleksandrov, Melkonyan & Stepanov (1984) and Cowan (1985). A pictorial model of the appropriate dispersion surface geometry, which is discussed at length below, has been developed by Baryshevskii (1976), Andreev *et al.* (1982) and Höche & Brümmer (1986). These dynamical treatments are similar to the earlier works on extremely asymmetric diffraction in which one of the external beams is nearly parallel to the surface, by Farwig & Shürmann (1967), Kishino (1971), Kishino, Noda & Kohra (1972), Bedynska (1973, 1974), Rustichelli (1975) and Härtwig (1976, 1977).

All of these efforts begin with the dynamical diffraction theory as originally formulated by Ewald (1916*a*, *b*, 1917) and later reformulated by von Laue (1931), in which a perfect crystal is represented by a periodic dielectric function (Batterman & Cole, 1964). In applying this theory to a specific scattering geometry, boundary conditions are imposed on the general solutions and certain approximations are made to simplify the equations. These analytic expressions are very useful for understanding the behavior of certain beams in particular geometries. Exact dynamical diffraction calculations can be performed by computer for any scattering geometry, however, using the completely general '*n*-beam' program developed by Colella (1974). The problem of solving for the wave vectors of all waves excited in a perfect crystal is reduced to the task of inverting and diagonalizing certain matrices, and the exact amplitudes of both the internal and external waves are then determined from the boundary conditions.

A. Dispersion surfaces and exit spheres

To describe the role of the dispersion surface in grazing-incidence geometries, we shall first review the two-beam dispersion surface picture of the symmetric Laue diffraction geometry for a parallel-sided thin perfect crystal whose surfaces are perpendicular to the plane of diffraction (Figs. 1*b* and 3). For waves inside the crystal, the dispersion surface is defined as all points in reciprocal space which can be the origin of pairs of plane wave vectors $(\mathbf{K}_O, \mathbf{K}_H)$ which are allowed solutions of the dynamical equations, whose tips lie at the point **O**, the origin of reciprocal space, and at **H**, the node of the reciprocal lattice responsible for diffraction. This surface can be approximated by two identical spheres centered on the points **O** and **H** which smoothly 'mix' at the plane of intersection to form two disconnected surfaces (Fig. 3). These two surfaces are known as the α and β branches, and their minimum separation in the plane of intersection is the Darwin width, whose magnitude is proportional to the strength of interaction between the X-rays and the crystal planes. (In the language of condensed-matter theory, these surfaces 'hybridize' at the Brillouin zone boundary and create a 'Bragg' band gap.)

In addition to the dispersion surfaces for interior waves, Fig. 3 also shows two larger circles about the **O** and **H** nodes which represent the origins of all possible wave vectors belonging to exit beams. Denoted L_O and L_H, the exit spheres have a radius $k = 1/\lambda$ where λ is the X-ray wavelength in vacuum (or air). The radius K of the dispersion surface 'spheres' away from the plane of intersection (*i.e.* away from the Bragg condition for strong diffraction, $|\mathbf{K}_O| = |\mathbf{K}_H|$) is smaller than k by a factor of κ, the dielectric constant, where $1 - \kappa$ is of the order of 10^{-5}.

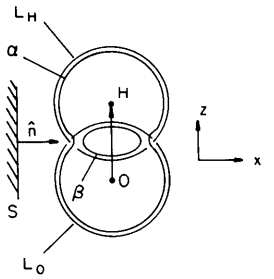

Fig. 3. Dispersion surfaces and exit spheres for symmetric two-beam Laue diffraction. The α and β surfaces associated with the **O** and **H** nodes are shown in cross section in the x–z diffraction plane. The larger circles about these nodes are cross sections of the L_O and L_H exit-beam spheres. The line S corresponds to the incident surface of the crystal, where $\hat{\mathbf{n}}$ is the surface normal vector. The actual internal waves and exit beams excited in a particular orientation are determined by the intersection of a line along $\hat{\mathbf{n}}$ with the dispersion surfaces and exit spheres. (The vertical position of $\hat{\mathbf{n}}$ here is set by having the intersection with L_O correspond to a wave vector parallel to the incident beam.) The separation between the exit spheres and the α surface has been greatly exaggerated for clarity.

To determine which wave vectors are actually excited for a particular scattering geometry, boundary conditions requiring phase continuity at the interfaces are imposed. This has been shown to be equivalent (Batterman & Cole, 1964) to drawing a vector $\hat{\mathbf{n}}$ along the crystal surface normal which intersects the L_O sphere at a position proportional to θ, the angle between the incident-beam wave vector and the (hkl) planes corresponding to **H**. The points of intersection of this line with the dispersion surfaces are called 'tie points', which are the origins of all allowed interior plane-wave vector pairs which connect **O** and **H** for the particular orientation of the crystal. Because the two plane waves associated with a tie point are coupled by $\mathbf{K}_H = \mathbf{K}_O + \mathbf{H}$, they act coherently to form a single wave field in the crystal. (These wave fields are precisely analogous to the Bloch wave fields which describe electron states in a crystal.) The intersections of $\hat{\mathbf{n}}$ with the exit spheres are called 'exit points', and determine the wave vectors of all exit beams propagating outside the crystal. An exit point on the **O** sphere, for example, is the origin of an exit wave vector which terminates at **O**.

The surface normal will generally intersect both dispersion surfaces twice, creating four tie points which excite four distinct wave fields inside the crystal, *i.e.* eight plane waves. Four of these plane waves propagate to the front (incident) surface and four propagate towards the rear surface. (The most general case would include two sets of dispersion surfaces, one set each for polarization vectors parallel and perpendicular to the diffraction plane, which leads to the excitation of up to eight internal wave fields. Without loss of generality, we restrict our attention to a single polarization state.) Maxwell's equations combined with the appropriate periodic dielectric function are required to determine the relative intensities of these waves. Of the four (eight) possible wave fields, typically only a few will have significant intensities unless θ is nearly equal to the Bragg angle.

For symmetric diffraction from a parallel-sided crystal, the external beams are determined by the exit points on the L_O and L_H spheres created by the same surface normal vector $\hat{\mathbf{n}}$ utilized above. A single incident beam can thus generate up to four exit beams, two from each surface. We denote the exit beams reflected from the incident surface by the symbols R_O and R_H, and the transmitted exit beams originating from the back surface are denoted T_O and T_H. For the symmetric Laue case considered here, these are the Laue diffracted beam (T_H), the Laue forward-diffracted beam (T_O), the Bragg diffracted beam (R_H) (which propagates antiparallel to the incident beam in this scattering geometry) and the specular reflected beam (R_O). The last two will have extremely small intensities for large angles of incidence.

We now turn our attention to symmetric Laue diffraction at grazing incidence, where the incident beam makes a small angle Φ with respect to the surface. The dispersion surfaces for interior waves are of course the same as before, but now the surface normal $\hat{\mathbf{n}}$ is nearly perpendicular to the diffraction plane (*i.e.* the plane containing the vector **H** and the incident beam). Fig. 4 shows an expanded three-dimensional view of the dispersion surfaces. The cross sections of the α and β surfaces in the x-z plane are the same as those shown in Fig. 3. The cross section in the x-y plane, consisting of two concentric circles, now contains the relevant portions of the dispersion surfaces since the crystal surface normal $\hat{\mathbf{n}}$ is parallel to the y axis.

The vector $\hat{\mathbf{n}}$ again can intersect four tie points for interior waves, exciting the eight wave vectors drawn in Fig. 4. Four of these waves propagate towards the back of the crystal and four towards the front, but all eight are travelling nearly parallel to the surface. We shall also see below that these eight waves, and thus all four exit beams, can each be strongly excited near grazing incidence over a small range of Φ and θ values.

We shall consider several cases in which the grazing angle Φ is varied while the angle θ made by the incident plane wave with respect to the **H** diffraction planes is fixed to certain values. Consider first a value of θ much less than θ_B, the Bragg angle. The cross section of the dispersion surface containing the surface normal $\hat{\mathbf{n}}$ is shown in Fig. 5(a), which consists of only the L_O and α circles. The vector $\hat{\mathbf{n}}$ intersects the L_O circle twice for finite values of Φ, indicating that both a specular* reflected beam R_O and a transmitted beam T_O can exit the specimen. For $\Phi < \Phi_c$, however, $\hat{\mathbf{n}}$ does not intersect the α branch, so travelling waves inside the crystal are not excited. The specular beam will therefore have nearly the same intensity as the incident beam, although for a sufficiently thin crystal a small amount of energy can 'leak' through to form a transmitted beam *via* excitation of evanescent waves. For $\Phi \gtrsim \Phi_c$ two tie points

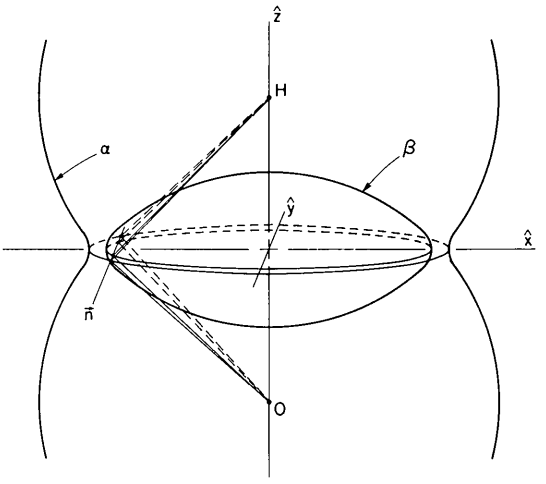

Fig. 4. Tie points and dispersion surfaces for glancing incidence diffraction. The α and β curves in the x-z plane are enlarged from Fig. 2. The surface normal $\hat{\mathbf{n}}$, however, is now perpendicular to the x-z plane, so the tie points of $\hat{\mathbf{n}}$ with the dispersion surfaces now lie in the x-y plane. The pertinent dispersion surface cross sections are now concentric α and β circles. In this figure $\hat{\mathbf{n}}$ corresponds to $\theta = \theta_B$ and a value of φ large enough to intersect both branches. These four tie points correspond to eight internal waves, whose wave vectors are indicated by the solid and dashed lines from the tie points to the nodes **O** and **H**. Note that all eight waves are propagating nearly parallel to the surface, with half travelling towards the front and half travelling towards the back of the crystal.

* Note that for $\theta \ll \theta_B$ the ratio of the radii of the L_O and α circles is κ, so

$$\cos\varphi \simeq \cos\Phi = \kappa,$$

in agreement with the usual derivations of the critical angle for non-diffracting geometries (*e.g.* James, 1982, p. 171).

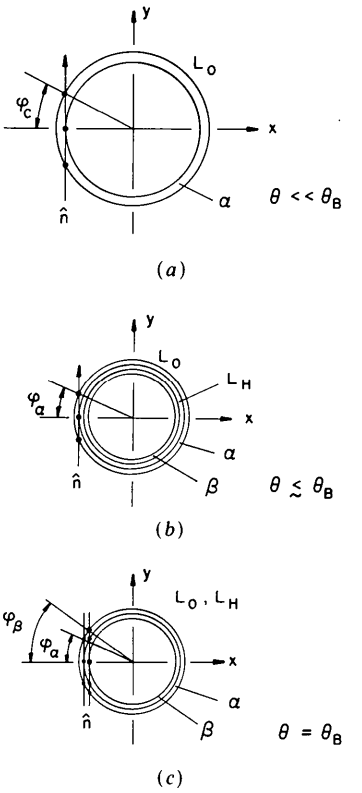

Fig. 5. Dispersion surface and exit beam circles for glancing incidence diffraction. (a) For $\theta \ll \theta_B$ the surface normal vector $\hat{\mathbf{n}}$ will only intersect the L_O sphere and the α branch of the dispersion surfaces. The critical angle φ_c corresponds to $\hat{\mathbf{n}}$ being tangent to the α circle. (b) For θ slightly less than θ_B, $\hat{\mathbf{n}}$ can intersect all four surfaces: L_O, α, L_H and β. For $\varphi = \varphi_\alpha$, $\hat{\mathbf{n}}$ is tangent to the α circle, which corresponds to the critical angle for exciting travelling waves into the crystal. (c) For $\theta = \theta_B$, the L_O and L_H circles are coincident. φ_α is the critical angle for exciting internal travelling waves on the α branch, and φ_β is the critical angle for the β branch.

on the α circle will be strongly excited, but the transmitted exit beam will quickly become more intense at the expense of the specular beam as Φ increases.* The transmitted-beam intensity will depend on the thickness of the crystal due to photoelectric absorption of the X-rays.

Next consider an angle θ only slightly smaller than θ_B. The dispersion surface cross section, depicted in Fig. 5(b), now includes the L_O, α, L_H and β branches. Only the specular exit beam R_O is strongly excited for $\Phi < \Phi_\alpha$ just as in the previous case, but note that Φ_α is less than Φ_c when θ is close to θ_B. For $\Phi_\alpha < \Phi < \Phi_H$ the transmitted exit beam T_O gains intensity, and the diffracted exit beams R_H and T_H become fully excited when $\Phi > \Phi_H$. The two tie points on the L_H circle correspond to the Bragg-diffracted beam R_H at the front surface and the Laue-diffracted beam T_H at the back surface, which can both be active since the α branch allows energy to flow through the crystal. The transmitted exit beam T_O now becomes the 'Laue forward-diffracted' beam. The two Laue beams T_O and T_H become more intense as Φ increases, especially when $\Phi > \Phi_\beta$ results in tie points on the β surface. (Note that for even smaller values of $\theta_B - \theta$ the L_H exit beam circle has a larger diameter than the α and β branches, so $\Phi_H < \Phi_\alpha < \Phi_\beta$.)

Although only the specular beam R_O is strongly excited for $\Phi < \Phi_\alpha$ in the above case, X-ray energy is present inside the crystal in the form of exponentially damped waves. These evanescent waves couple to the α and β branches of the dispersion surfaces, and to the L_H exit-beam sphere. Since the direction of energy flow associated with the specular beam is parallel to the surface (neglecting absorption), the waves near the surface corresponding to evanescent excitations of the α, β and/or L_H circles also propagate parallel to the surface. Since a tie point on the α and β surfaces corresponds to the origin of two wave vectors, and an exit point on the L_H exit-beam circle corresponds to one wave vector, up to five evanescent waves may participate in specular reflection near the Bragg angle. This topic has been extensively discussed by Andreev *et al.* (1982), Cowan (1985) and Cowan *et al.* (1986).

When the angle θ is exactly equal to the Bragg angle θ_B, the L_O and L_H circles are coincident, as shown in Fig. 5(c). The diffracted **H** beams R_H and T_H can therefore be excited for all values of Φ. Since interior travelling waves are not excited for $\Phi < \Phi_\alpha$, only the Bragg-diffracted beam R_H and the specular reflected beam R_O will have significant intensity. The intensities of these two beams calculated with the exact 'n-beam' procedure described below are plotted as a function of φ in Fig. 6. Note that nearly all of the incident-beam intensity is shared between these two beams for $\varphi < \varphi_\alpha$, with the Bragg-diffracted beam R_H starting at zero and growing to nearly $\sim 0{\cdot}5 I_0$ at $\varphi = \varphi_\alpha$. For $\varphi_\alpha < \varphi < \varphi_\beta$, however, a significant fraction of the incident intensity is no longer present in the reflected beams. The excitation of α branch tie points produces internal waves travelling away from the front surface, which couple some of the missing intensity to the Laue beams T_O and T_H at the back surface of the crystal. (The remainder is absorbed by the crystal.) For $\varphi > \varphi_\beta$ the specular and Bragg-diffracted beams R_O, and R_H quickly die out.

Similar excitation processes occur for angles θ greater than θ_B. Since the L_H circle will now have a diameter larger than the L_O circle, there will be two exit points intersected on the L_H circle for all values of Φ. The diffracted exit beams therefore cannot be evanescent.

B. Colella's matrix formulation of dynamical diffraction

The amplitude and direction of all plane waves generated inside a perfect crystal for a particular scattering geometry are determined by Maxwell's equations for electromagnetic waves propagating in a medium with a spatially periodic dielectric function. The resulting set of coupled equations can be reduced to the following form [Colella (1974), following Zachariasen (1945)]:

$$(k^2 - K_i^2)\mathbf{D}_i - \sum_{j=1}^{n} \Psi_{i-j}[(\mathbf{K}_i \cdot \mathbf{D}_j)\mathbf{K}_i - K_i^2 \mathbf{D}_j] = 0 \quad (1)$$

where $\mathbf{K}_j$ is the wave vector associated with the jth

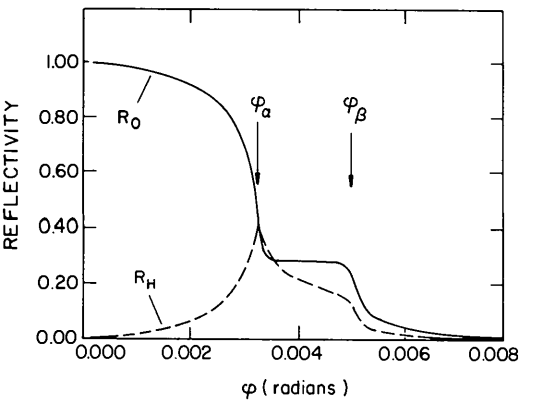

Fig. 6. Reflectivity profiles calculated with the 'n-beam' program (Colella, 1974). The intensities of the R_O specular beam and the R_H Bragg diffracted beam are calculated for a $(11\bar{1})$ silicon surface with $\mathbf{H} = [220]$. These curves are φ scans for a constant $\theta = \theta_B$, with an X-ray energy of 8·0 keV. The intensities are normalized to the incident-beam intensity.

* How strongly a tie point is excited cannot be determined from just the dispersion surface, which only selects those wave vectors which are allowed by conservation of energy and wave momentum. The actual intensities of the allowed waves must be determined by applying boundary conditions to the solutions of the dynamical equations. The statement that the tie point coupled to the specular beam is less strongly excited at larger angles of incidence, for example, is easily proven from the Fresnel boundary conditions.

node of the reciprocal lattice, $\mathbf{D}_j$ is the complementary displacement vector and Ψ_j is the jth Fourier component of the polarizability per unit volume times 4π. (Note that the polarizability components Ψ_j are proportional to the usual structure factors F_j, which are the Fourier components of the electron density.) The index $i = 1, 2, \ldots, n$ corresponds to those nodes of the reciprocal lattice which contribute to the diffraction, so (1) is actually a set of n coupled vector equations.

For the simple case where the incident X-ray beam strongly interacts with only a single set of (hkl) planes corresponding to the reciprocal-lattice vector $\mathbf{H}$, only two equations containing the origin $\mathbf{O}$ and the node $\mathbf{H}$ have solutions with significant intensities:

$$\begin{aligned}[k^2-(1-\Psi_O)K_O^2]\mathbf{D}_O+\Psi_{\bar{H}}K_O^2 D_H &= \Psi_{\bar{H}}(\mathbf{K}_O \cdot \mathbf{D}_H)\mathbf{K}_O \\ \Psi_H K_H^2 \mathbf{D}_O+[k^2-(1-\Psi_O)K_H^2]\mathbf{D}_H &= \Psi_H(\mathbf{K}_H \cdot \mathbf{D}_O)\mathbf{K}_H.\end{aligned} \tag{2}$$

The solutions of (1) are discussed at length by Colella (1974). If we assume the existence of a wave with a particular wave vector $\mathbf{K}_O$ inside an infinite perfect crystal, then the equations give the relative amplitudes and wave vectors of all other waves which are simultaneously excited by the $\mathbf{K}_O$ wave. For a parallel-sided crystal with an external plane wave beam incident upon the front surface at an angle Φ and also making an angle θ with respect to a particular set of (hkl) planes, the allowed waves are determined by applying Fresnel boundary conditions at both surfaces. Phase continuity requires that the tangential components of the electric and magnetic field amplitudes and the normal components of the electric displacement and magnetic induction amplitudes be conserved at the interfaces. The imposition of these boundary conditions is the mathematical equivalent of determining the tie points of the dispersion surfaces and the exit points of the exit beam spheres using the surface normal vector $\hat{\mathbf{n}}$, as described above.

Equations (1) and (2) with the appropriate boundary conditions for symmetric diffraction will describe four exit beams, two Bragg beams at the front surface and two Laue beams at the back surface. In most scattering geometries the only measurable exit beams for a particular $\mathbf{H}$ reflection will be either Bragg or Laue, but not both. $\mathbf{H}$ is then referred to as either a Bragg reflection or a Laue reflection. Equations (1) and (2) can be correspondingly simplified (linearized) in a manner which eliminates the two exit beams of negligible intensity. This is done in traditional descriptions of dynamical theory, and is perfectly justified for most applications. As was first pointed out by Colella (1974), however, a reflection $\mathbf{H}$ which excites beams travelling parallel to a surface can have interior wave components directed towards either surface of the crystal. Such a reflection can excite both Bragg *and* Laue beams, so the simplified equations which throw out half of the exit beam solutions will not always be adequate. Colella has shown how (1) can be exactly solved by inverting one $2n \times 2n$ matrix and diagonalizing another $4n \times 4n$ matrix, where n is the number of nodes of the reciprocal lattice which contribute to diffraction, and both polarization states are included.

The n-beam matrix description of dynamical diffraction is especially powerful when the X-rays are interacting with more than one set of (hkl) planes, *i.e.* for $n > 2$. [For examples, see Colella (1974), Tischler & Batterman (1986), and Schmidt & Colella (1985).] For the relatively simple case considered here where only the $\mathbf{O}$ and $\mathbf{H}$ nodes contribute ($n = 2$), the n-beam approach is essential to treat exactly the simultaneous Bragg and Laue contributions. An additional benefit of the n-beam approach is that the same computer program can be used without modification to determine the diffracted waves for any value of Φ and θ, ranging from the grazing incidence considered here ($\Phi < \Phi_c$) to normal incidence Bragg angles ($\theta_B \simeq \pi/2$) (Colella & Luccio, 1984).

III. Experimental results and comparison with theory

We have performed X-ray measurements on a thin slab of nearly perfect silicon which illustrate the coupling between Laue and Bragg beams for grazing-incidence geometries. We show that the qualitative behavior is described well by the geometrical dispersion surface picture given above, and that this Bragg–Laue regime can be quantitatively modelled with Colella's exact matrix formulation of dynamical diffraction.

The specimen was a 5·0 cm diameter silicon wafer, commercially obtained with a standard mirror-like finish on both sides and a thickness of 0·20 mm. The surfaces were parallel to {111} planes, so there were {220} planes perpendicular to the surfaces which provided the reciprocal-lattice vector $\mathbf{H} = [220]$ in the plane of the surface. The 220 reflection was selected for all diffraction measurements in part because it is a 'full' reflection, *i.e.* all atoms in the unit cell scatter in phase, which minimizes the absorption of the α-branch waves in the crystal near the Bragg angle.

The specimen was briefly etched in a 95% HNO_3–5% HF solution to remove excess surface oxides. A thin film of AuPd alloy approximately 40 Å thick was sputtered onto one face of the wafer.* X-ray fluorescence from this layer was intended to serve as a detector of diffracted X-ray intensity at this surface, especially in the regime where the T_H beam is

* The authors are indebted to J. Liu and N. Giordano at Purdue University for sputtering the AuPd layer onto the specimen.

evanescent. These measurements proved not to be very revealing in themselves, but the AuPd layer did have a somewhat unexpected effect on the reflected surface diffraction beams, as described below.

This crystal was mounted on a four-circle diffractometer with the [220] direction aligned with the φ axis, at the A-3 experimental station at the Cornell High Energy Synchrotron Source (CHESS). Synchrotron radiation was monochromated by a (220) silicon double-crystal monochromator which was normally detuned slightly to reduce the $\lambda/2$ content of the beam. The specimen was oriented such that a 220 reflection diffracted the monochromated beam in a non-dispersive manner. The incident beam was reduced by horizontal slits to a width of 0·075 mm, and the full vertical height of the beam (about 5 mm) was employed. The flux reaching the specimen was typically about 10^7 photons s^{-1}.

Diffraction scans were usually made by keeping the incident angle φ fixed while scanning the angle θ through the 220 reflection. For values of φ near the critical angle φ_c, both the Laue diffracted beam T_{220} and the nearly parallel Bragg reflected beam R_{220} could be excited for slightly different values of θ. A single wide-open scintillation detector was positioned to measure simultaneously both of these diffracted beams. An example of such a measurement is given in Fig. 7, where $\varphi = 0{\cdot}73°$ and the X-ray energy is 11·95 keV. Note that these data include broadening due to both the monochromator transmission function and the horizontal divergence of the synchrotron radiation. This plot shows at once that a single node **H** can produce Bragg and Laue beams.

It is well known for ordinary scattering geometries ($\varphi \gg \varphi_c$) that Bragg's law

$$n\lambda = 2d_{hkl} \sin \theta_B$$

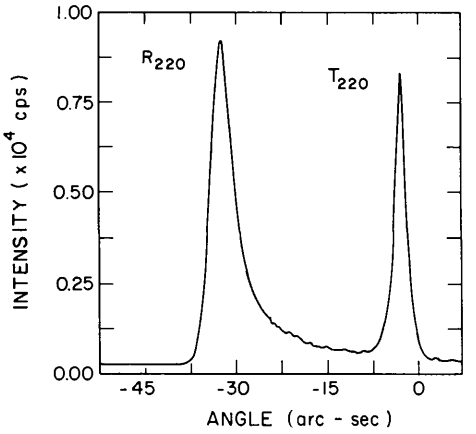

Fig. 7. Measured [220] Bragg and Laue diffracted beams. An 11·95 keV (1·04 Å) X-ray beam is incident to the $(11\bar{1})$ silicon wafer surface at $\varphi = 0{\cdot}75°$, while the diffraction angle θ is scanned near θ_B for the 220 reflection. A single detector is measuring both beams.

holds exactly for symmetric Laue reflections, but must be modified to include a small refractive shift $\delta\theta$ for Bragg reflections (Batterman & Cole, 1964):

$$n\lambda = 2d_{hkl} \sin (\theta_B + \delta\theta).$$

The size of this shift is of the order of the intrinsic Darwin width of the reflection, and depends on the average electron density (*i.e.* the **O** Fourier component of the electron scattering density). At grazing incidence the Laue diffracted beam T_H still occurs at exactly θ_B, but the shift in the Bragg diffracted beam R_H is now a function of φ, and can be much larger than the usual refractive shift. Note that measuring both the Laue and the Bragg diffracted beams in a single scan provides a precise value for this shift, since the Laue beam T_H serves as a fiducial reference for θ_B.

We can use our geometrical picture of the dispersion surfaces and the exit spheres to show the relationship between $\delta\theta \equiv \theta - \theta_B$ and the angle φ. In Fig. 8(*a*) a cross section of the L_O and L_H exit spheres is shown for a small value of $\delta\theta$. The surface normal $\hat{\mathbf{n}}$ is drawn for a particular incident beam φ, which intersects an exit point on the L_H circle indicating a different angle φ' for the Bragg diffracted beam R_H. Note that

$$r_O \cos \varphi = r_H \cos \varphi' \tag{3}$$

where r_O and r_H are the radii of the L_O and L_H exit circles. From Fig. 8(*b*) it is seen that, for small values of $\delta\theta$,

$$\begin{aligned} r_O &= k \cos (\theta_B + \delta\theta) \\ r_H &= k \cos (\theta_B - \delta\theta). \end{aligned} \tag{4}$$

Combining these two results and treating φ, φ' and $\delta\theta$ as small quantities, we have*

$$\varphi'^2 = \varphi^2 + 4\delta\theta \tan \theta_B. \tag{5}$$

Finally we need to impose a condition which should correspond to the peak intensity of the Bragg reflected beam R_H. Note that in general there are two exit points on the L_H circle. For φ larger than φ_α this can lead to both Laue and Bragg beams. We find empirically that choosing $\delta\theta$ (for a given φ) such that $\varphi' = 0$

* It can be shown that this result is equivalent to equation (3) of Afanas'ev & Melkonyan (1983):

$$\varphi^2 = \varphi'^2 + \alpha, \tag{3}$$

where

$$\alpha = [(\mathbf{k}_O + \mathbf{H})^2 - k^2]/k^2.$$

Similarly, this result can also be compared with equation (3) of Cowan (1985):

$$k_{H\perp} = \pm k(\Phi^2 + 2y)^{1/2} \tag{3}$$

where $y = \delta\theta \sin 2\theta_B$. Substituting $k\Phi' = k_{H\perp}$ and squaring yields

$$\Phi'^2 = \Phi^2 + 2\delta\theta \sin 2\theta_B.$$

This can be derived from equation (5) above by noting again that

$$\sin \Phi = \sin \varphi \cos \theta.$$

will correspond approximately to the peak in the Bragg reflected beam. That is, we choose $\hat{\mathbf{n}}$ so that it is tangent to the L_H circle, exciting only one exit point. This observation is borne out by the results of numerical calculations, as noted below.

We can use this result to determine the value of φ for each θ scan, which can be difficult to determine accurately with the experimental apparatus. We assume that the Bragg reflected peak positions correspond to $\varphi' = 0$, so

$$\varphi = (-4\delta\theta \tan \theta_B)^{1/2}.$$

We plotted the nominal values of φ *versus* $(-4\delta\theta \tan \theta_B)^{1/2}$ for 15 θ scans at different φ values, and found that the data were fit well by a straight line. The intercept of this line at $\delta\theta = 0$ determines the origin of the φ axis, which provided a correction to the nominal values of φ. These data with the proper φ axis are shown in Fig. 9.

A set of θ scans corresponding to three of the points in Fig. 8 is presented in Fig. 10. Plotted together are the (Bragg) R_{220} and (Laue) T_{220} peaks for φ values of 0·53, 0·73 and 0·88° for an X-ray energy of 11·95 keV ($\lambda = 1{\cdot}04$ Å). Note that the Laue peaks show no significant shift in θ, whereas the Bragg peaks are displaced from θ_B by amounts which are many times larger than the Darwin widths. (Slight variations in the Laue peak position and line shape are expected due to the changing α and β contributions as a function of φ.) The values of $\theta - \theta_B$ match well the predictions of the geometrical dispersion surface-exit sphere picture, a conclusion which can also be drawn from the straight-line fit in Fig. 9.

The *n*-beam program was used to generate theoretical curves for the appropriate values of φ and θ, and the results are plotted in Fig. 10. Considering that the data are broadened by both the horizontal divergence of the synchrotron and the double monochromator transmission function, we feel that the general agreement between theory and experiment for the position and intensity of the diffraction peaks is fairly good. Since there can be little doubt of the accuracy of the *n*-beam program, this agreement can be taken as verification that the specimen was of high quality and that the measured values of $\theta - \theta_B$ and φ were accurate. More generally, these three θ scans demonstrate how the diffracted intensity gradually shifts from the Laue beam to the Bragg beam as φ is diminished, although there is a large span of φ (many times larger than φ_c) over which both beams have considerable intensity.

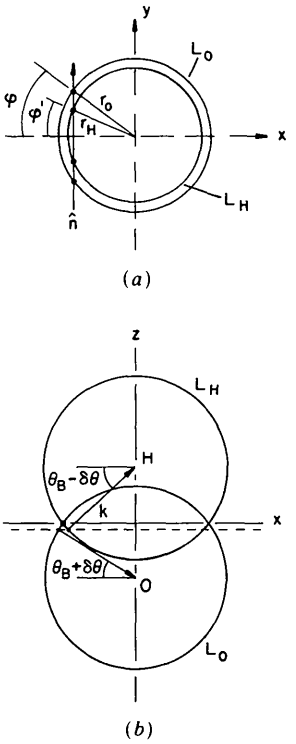

Fig. 8. Exit-sphere diagrams for determining Bragg diffracted (R_H) beam exit angle φ'. (*a*) The cross section of the L_O and L_H exit spheres is shown for θ slightly less than θ_B, where L_O has a radius r_O and L_H has a radius r_H. The incident beam makes the glancing angle φ to the entrance surface, while the R_H beam makes the angle φ', as indicated by the exit points. (*b*) View of the exit surfaces in a plane containing **H**. The deviation from θ_B is $\delta\theta$. Note that the dashed line indicates the plane shown above in part (*a*). The radius of the exit spheres is $k = 1/\lambda$, where λ is the X-ray wavelength in vacuum.

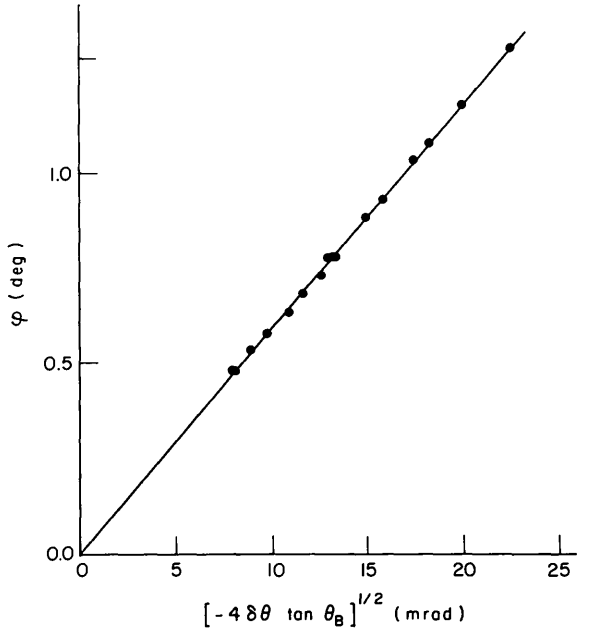

Fig. 9. Plot of the measured separation of the Bragg and Laue diffracted beams. Fifteen θ scans similar to that shown in Fig. 6 were obtained for various values of glancing angle φ. The φ for each scan is plotted against the quantity $[-4\delta\theta \tan \theta_B]^{1/2}$, where $\delta\theta = \theta - \theta_B$ is the measured angle between Bragg and Laue diffracted beams. The straight-line fit is consistent with the geometrical model illustrated in Fig. 8.

All of the above measurements were made with the incident X-ray beam striking the clean silicon surface, *i.e.* the back surface had the 40 Å sputtered layer of AuPd alloy. This metal film has a negligible effect on the Laue beam intensities, and no effect at all on the Laue angle θ_B, so its presence has been ignored so far. The situation was quite different, however, when the X-ray beam was incident upon the AuPd surface. The R_H Bragg reflected beam could no longer be detected, although the R_O specular beam and the T_O and T_H Laue beams were all present as before.

This unanticipated result can be explained by treating the thin AuPd film as a continuous medium whose dielectric constant is smaller than that of silicon or of air (*i.e.* $\kappa_{AuPd} < \kappa_{Si} < \kappa_{air} \simeq 1$). This is expected from the greater electron density in AuPd. External reflection of the R_O and R_H beams at an air-silicon interface is a consequence of the X-ray wavelength ($\lambda = 1/\kappa$) in silicon being longer than the wavelength in air. At the AuPd-Si interface, the wavelength in silicon is *shorter* than the wavelength in AuPd, so external reflection is not possible. The observed R_O specular beam is simply that externally reflected from the air-AuPd interface. Because the AuPd layer is so thin, much of the incident intensity is transmitted to the silicon interface, even for $\Phi < \Phi_c^{Au}$. This intensity will excite travelling waves inside the silicon, which couple to the T_O and T_H Laue beams at the back surface.

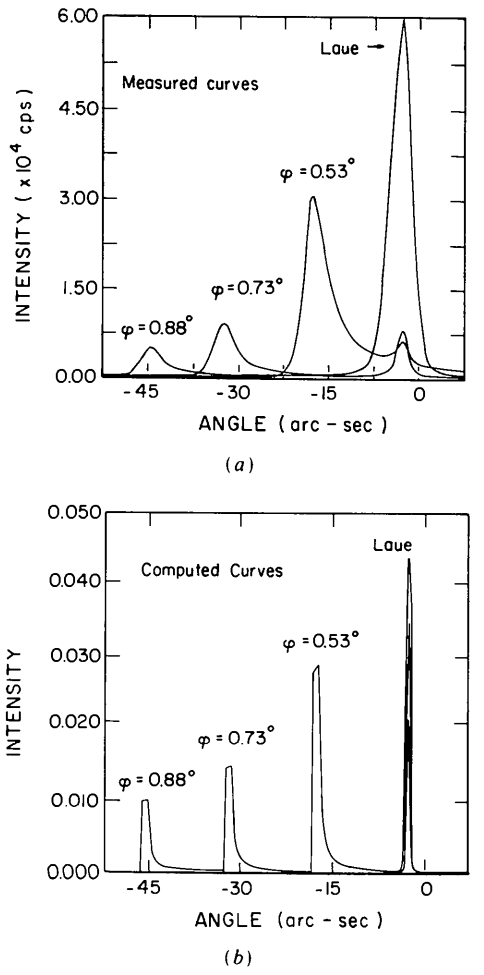

Fig. 10. Comparison of the experimental Bragg-Laue curves with the '*n*-beam' theory. (*a*) The three measured curves showing both the Bragg R_{220} beam and the Laue T_{220} beam as a function of $\delta\theta$ were obtained for glancing angles $\varphi = 0{\cdot}530$, $0{\cdot}73$ and $0{\cdot}88°$. (*b*) The calculated curves are generated by the *n*-beam program for these φ values. The measured intensities are each multiplied by the same arbitrary scale factor. The discontinuous drop on the low-angle side of the calculated R_{220} curves corresponds to the beam becoming evanescent.

What is perhaps surprising is the apparent bulk-like nature of this 40 Å sputtered film with respect to its X-ray dielectric properties. The silicon wafer had been chemically polished and etched before the deposition, but the surface was undoubtedly rough on a microscopic scale and had to include some superficial silicon oxide. The 40 Å overlayer must also be rough and probably discontinuous, although the AuPd alloy was chosen for its well known tendency for forming continuous films at somewhat greater thicknesses. Despite these imperfections, the lack of a Bragg diffracted beam necessarily indicates the presence of an interface between silicon and a material with an effective dielectric constant less than that of silicon (*i.e.* the effective electron density had to be greater in the overlayer than in the silicon). The naturally occurring surface oxide layer does not have a similar effect on surface diffraction because the dielectric constant of silicon oxides is larger than that of silicon, although Bernhard *et al.* (1987) have shown that surface diffracted profiles are weakly influenced by the oxide layer.

IV. Concluding remarks

We have demonstrated both experimentally and theoretically that grazing-incidence diffraction from planes perpendicular to a crystal surface leads to both Bragg and Laue exit beams. The data from synchrotron-based measurements of a thin (111) silicon wafer can be qualitatively understood by constructing dispersion surface diagrams appropriate for a grazing-incidence geometry. In particular, the large splitting in θ values observed for the Bragg and Laue diffracted beams for various grazing angles were quite accurately described by (5), which was derived from geometrical considerations. The exact *n*-beam theory of Colella (1974) was shown to describe accurately grazing-incidence Bragg-Laue X-ray diffraction, a further example of the power and versatility of the *n*-beam program.

This work extends many previous treatments of semi-infinite perfect crystals to the case of a crystal slab of finite thickness. In general the previously derived results (Afanas'ev & Melkonyan, 1983;

Cowan, 1985) for Bragg beams carry over to the thin-crystal case considered here. One important exception, however, occurs when the θ values of the Bragg and Laue diffracted beams are very close together (*i.e.* for $\Phi < \Phi_c$). In this case the strongly excited internal waves travelling towards the rear surface to generate the Laue exit beams are also partially reflected back towards the front surface. These waves can then contribute to the intensity of the Bragg exit beams, although in practice this effect is usually negligible. Calculating the magnitude of these 'internally reflected Laue waves' requires a method such as the n-beam theory which retains all of the solutions of the dynamical equations.

We are grateful for the expert assistance of the staff of the Cornell High Energy Synchrotron Source (CHESS) during the X-ray measurements, and we thank Professor R. Colella for a copy of his n-beam program and for helpful conversations. One of us (TG) acknowledges the support of a David Ross Fellowship. This work was supported by the National Science Foundation through Grant No. DMR-8703993.

References

AFANAS'EV, A. M. & MELKONYAN, M. K. (1983). *Acta Cryst.* A**39**, 207-210.

ALEKSANDROV, P. A., MELKONYAN, M. K. & STEPANOV, S. A. (1984). *Kristallografiya*, **29**, 376. Engl. transl: *Sov. Phys. Crystallogr.* **29**, 226.

ANDREEV, A. V., KOV'EV, E. K., MATVEEV, Y. A. & PONOMAREV, Y. V. (1982). *Pis'ma Zh. Eksp. Teor. Fiz.* **35**, 412. Engl. transl: *JETP Lett.* **35**, 508.

BARYSHEVSKII, V. G. (1976). *Pis'ma Zh. Tekh. Fiz.* **2**, 112. Engl. transl: *Sov. Tech. Phys. Lett.* **2**, 43.

BATTERMAN, B. W. & COLE, H. (1964). *Rev. Mod. Phys.* **36**, 681-717.

BEDYNSKA, T. (1973). *Phys. Status Solidi A*, **19**, 365-372.

BEDYNSKA, T. (1974). *Phys. Status Solidi A*, **25**, 405-411.

BERNHARD, N., BURKEL, E., GOMPPER, G., METZGER, H., PEISL, J., WAGNER, H. & WALLNER, G. (1987). *Z. Phys. B*, **69**, 303-311.

COLELLA, R. (1974). *Acta Cryst.* A**30**, 413-423.

COLELLA, R. & LUCCIO, A. (1984). *Opt. Commun.* **50**, 41-44.

COWAN, P. L. (1985). *Phys. Rev. B*, **32**, 5437-5439.

COWAN, P. L., BRENNAN, S., JACH, T., BEDZYK, M. J. & MATERLIK, G. (1986). *Phys. Rev. Lett.* **57**, 2399-2402.

EWALD, P. P. (1916*a*). *Ann. Phys. (Leipzig)*, **49**, 1-38.

EWALD, P. P. (1916*b*). *Ann. Phys. (Leipzig)*, **49**, 117-143.

EWALD, P. P. (1917). *Ann. Phys. (Leipzig)*, **54**, 519-597.

FARWIG, P. & SCHÜRMANN, H. W. (1967). *Z. Phys.* **204**, 489-500.

HÄRTWIG, J. (1976). *Phys. Status Solidi A*, **37**, 417-425.

HÄRTWIG, J. (1977). *Phys. Status Solidi A*, **42**, 495-500.

HÖCHE, H. R. & BRÜMMER, O. (1986). *Acta Cryst.* A**42**, 585-587.

JAMES, R. W. (1982). *The Optical Principles of the Diffraction of X-rays.* Woodbridge, Connecticut: Ox Bow Press.

KISHINO, S. (1971). *J. Phys. Soc. Jpn*, **31**, 1168-1173.

KISHINO, S., NODA, A. & KOHRA, K. (1972). *J. Phys. Soc. Jpn*, **33**, 158-166.

LAUE, M. VON (1931). *Ergeb. Exakten Naturwiss.* **10**, 133-158.

LORRAIN, P. & CORSON, D. (1970). *Electromagnetism and Waves.* San Francisco: Freeman.

MARRA, W. C., EISENBERGER, P. & CHO, A. Y. (1979). *J. Appl. Phys.* **50**, 6927-6933.

RUSTICHELLI, F. (1975). *Philos. Mag.* **31**, 1-12.

SCHMIDT, M. & COLELLA, R. (1985). *Phys. Rev. Lett.* **55**, 715-717.

TISCHLER, J. & BATTERMAN, B. W. (1986). *Acta Cryst.* A**42**, 510-514.

VINEYARD, G. (1982). *Phys. Rev. B*, **26**, 4126-4159.

ZACHARIASEN, W. H. (1945). *Theory of X-ray Diffraction in Crystals.* New York: John Wiley.

SHORT COMMUNICATIONS

Contributions intended by publication under this heading should be expressly so marked; they should not exceed about 1000 *words; they should be forwarded in the usual way to the appropriate Co-editor; they will be published as speedily as possible.*

Acta Cryst. (1989). A**45**, 141-143

A new von Mises probabilistic formula for quartet invariants.

By C. GIACOVAZZO, *Dipartimento Geomineralogico, Università, Campus Universitario,* 70124 *Bari, Italy,* and M. CAMALLI and R. SPAGNA, *Istituto di Strutturistica Chimica 'G. Giacomello', CNR, CP*10, *Monterotondo Stazione,* 00016 *Roma, Italy*

(*Received* 27 *January* 1988; *accepted* 19 *July* 1988)

Abstract

Von Mises formulas for quartet invariants [Giacovazzo (1976). *Acta Cryst.* A**32**, 91-99], even if useful in most cases of practical interest, suffer from some systematic errors. A new von Mises formula is suggested with better theoretical features.

Symbols

$\Phi = \varphi_{\mathbf{h}} + \varphi_{\mathbf{k}} + \varphi_{\mathbf{l}} - \varphi_{\mathbf{h}+\mathbf{k}+\mathbf{l}}$

$R = |E|$

$\varepsilon = R^2 - 1$

$E_{\mathbf{l}} = R_{\mathbf{l}} \exp(i\varphi_{\mathbf{l}}) = E_{\mathbf{h}} \exp(i\varphi_{\mathbf{h}})$;

0108-7673/89/010141-03$03.00